RSC Advances

PAPER

View Article Online
View Journal | View Issue

Cite this: *RSC Adv.*, 2017, **7**, 34538

Catalytic effect of $(Ti_{0.85}Zr_{0.15})_{1.05}Mn_{1.2}Cr_{0.6}V_{0.1}Cu_{0.1}$ on hydrogen storage properties of ultrafine magnesium particles†

Peng Liu,[a] Xiujuan Ma,[a] Xiubo Xie,[a] Xingguo Li[b] and Tong Liu *[a]

Received 15th May 2017
Accepted 2nd July 2017

DOI: 10.1039/c7ra05461k

rsc.li/rsc-advances

In order to improve hydrogen storage properties of magnesium, $(Ti_{0.85}Zr_{0.15})_{1.05}Mn_{1.2}Cr_{0.6}V_{0.1}Cu_{0.1}$ ($TiMn_2$ type) alloy particles have been added into magnesium ultrafine particles produced by a hydrogen plasma-metal reaction approach by ball milling. The $(Ti_{0.85}Zr_{0.15})_{1.05}Mn_{1.2}Cr_{0.6}V_{0.1}Cu_{0.1}$ particles are uniformly dispersed on the surface of magnesium. The addition of $(Ti_{0.85}Zr_{0.15})_{1.05}Mn_{1.2}Cr_{0.6}V_{0.1}Cu_{0.1}$ alloy improves both the hydrogen storage capacity and kinetics of magnesium. The magnesium–5 wt% $(Ti_{0.85}Zr_{0.15})_{1.05}Mn_{1.2}Cr_{0.6}V_{0.1}Cu_{0.1}$ composite can absorb 6.00 wt% H_2 within 60 minutes at 523 K and desorb 6.00 wt% H_2 within 15 minutes at 623 K. With the increase of $(Ti_{0.85}Zr_{0.15})_{1.05}Mn_{1.2}Cr_{0.6}V_{0.1}Cu_{0.1}$, the hydrogenation and dehydrogenation kinetics of the composites improve. The apparent activation energies of magnesium–*x* wt% $(Ti_{0.85}Zr_{0.15})_{1.05}Mn_{1.2}Cr_{0.6}V_{0.1}Cu_{0.1}$ ($x = 5$, 10, 30) composites for hydrogen absorption and desorption are 67.52, 65.80, 60.99 kJ mol^{-1} and 121.37, 116.68, 77.25 kJ mol^{-1}, respectively. The enhanced hydrogen storage capacities and kinetics can be attributed to the effective catalysis of the $(Ti_{0.85}Zr_{0.15})_{1.05}Mn_{1.2}Cr_{0.6}V_{0.1}Cu_{0.1}$ alloy and ultrafine size of magnesium particles.

Introduction

With fossil fuel resources rapidly depleting, searching for alternative energy resources is becoming an increasingly common concern for governments and scientists worldwide. Hydrogen, as a kind of pollution-free, high-energy-density and recyclable secondary energy carrier, is one of the most promising candidates to substitute fossil fuels in the future. Conventional storage of compressed hydrogen under high pressure is of low gravimetric and volumetric H_2 density, making it difficult to reach the targets of the DOE.[1] Meanwhile, storage of liquid hydrogen faces problems of nearly 30% energy loss in the process of liquefaction and the high requirements for the storage system. Compared with these methods, storing hydrogen using solid-state materials has the advantages of suitable storage capacity, high safety and less energy loss.[2,3] Among various solid-state hydrogen storage materials, magnesium (Mg) is considered to be an attractive one for its high theoretical reversible hydrogen storage capacity (7.6 wt%), light weight and low cost.[4,5] However, the sluggish hydrogenation/dehydrogenation kinetics and the high decomposition temperature still limit its practical application for hydrogen storage.[6]

Transition metals,[7,8] oxides[9–13] and hydrogen storage alloys[14,15] were used as the catalysts to improve the hydrogen storage performance of Mg through ball milling technique. Among these additives, hydrogen storage alloys which can absorb and desorb hydrogen at room temperature are quite potential one for their effective catalysts on kinetics and hydrogen capacities. Generally, Mg could absorb hydrogen only at temperatures higher than 573 K with a slow hydrogenation rate. It has been reported that Mg at microscale absorbed 1.5 wt% H_2 within 2 h at 673 K.[16,17] The milled Mg–$TiMn_{1.5}$ composite absorbed hydrogen of 4.0 wt% at 573 K in 5 min.[18] A milled Mg–$Ti_{0.28}Cr_{0.50}V_{0.22}$ composite could absorb 4.0 wt% H_2 at 548 K within 10 min.[19] After ball milling for 5 hours, the Mg–$V_{0.855}Ti_{0.095}Fe_{0.05}$ composite presented a rapid hydrogen sorption rate, which was able to uptake 4.97 wt% H_2 at 573 K within 60 min and release 5.5 wt% hydrogen at 623 K within 40 min.[20] Among the hydrogen storage alloys, the $TiMn_2$ type alloys[21] with excellent hydrogen storage properties at room temperature are seldom studied as an additive for Mg-based hydrogen storage material, let alone the consideration of their content on the performance of Mg.

Although high energy ball milling can reduce the grains of Mg particles to nanosize, their particle sizes are still in the range of micrometers.[22,23] It has been demonstrated that the sorption kinetics of Mg can be significantly enhanced when its size is reduced to nanoscale.[24–29] Thus, using Mg ultrafine particles (UFPs) and doping $TiMn_2$ type alloys are expected to improve

[a]*Key Laboratory of Aerospace Materials and Performance, Ministry of Education, School of Materials Science and Engineering, Beihang University, No. 37 Xueyuan Road, Beijing, 100191, China. E-mail: tongliu@buaa.edu.cn; Fax: +86 10 82316192; Tel: +86 10 82316192*

[b]*Beijing National Laboratory for Molecular Sciences (BNLMS), The State Key Laboratory of Rare Earth Materials Chemistry and Applications, College of Chemistry and Molecular Engineering, Peking University, Beijing 100871, China*

† Electronic supplementary information (ESI) available. See DOI: 10.1039/c7ra05461k

the comprehensive hydrogen storage performance of Mg. Hydrogen plasma-metal reaction (HPMR) approach is often used to produce metallic UFPs at large scale and with high purity. Recently, Mg and Mg-based composite UFPs, such as Mg–Al, Mg–Ti–V, and Mg–Nb, have been successfully prepared through HPMR technique.[30–32] Recently, we prepared a kind of $TiMn_2$ type alloy ($(Ti_{0.85}Zr_{0.15})_{1.05}Mn_{1.2}Cr_{0.6}V_{0.1}Cu_{0.1}$) with good hydrogen storage properties at room temperature. In this work, we intend to fabricate the Mg–x wt% $TiMn_2$ (x = 0, 5, 10, 30) composites by milling the Mg UFPs produced by HPMR with the $TiMn_2$ alloy, investigate their hydrogen storage properties and the effects of content of $TiMn_2$ alloy on the performance of Mg, and clarify the catalytic mechanism of the $TiMn_2$ alloy for improving the hydrogenation and dehydrogenation properties of Mg in detail.

Experimental

Preparation of Mg–x wt% $(Ti_{0.85}Zr_{0.15})_{1.05}Mn_{1.2}Cr_{0.6}V_{0.1}Cu_{0.1}$ composites

The $(Ti_{0.85}Zr_{0.15})_{1.05}Mn_{1.2}Cr_{0.6}V_{0.1}Cu_{0.1}$ alloy was prepared by arc melting of the constituent metals with the purity more than 99.5% on a water-cooled copper crucible under a high purity argon atmosphere (99.999%). An excess amount of Mn of 5 wt% was added considering the weight loss of Mn during melting due to its low melting point. The button was turned over and re-melted four times to ensure high homogeneity. Then, it was mechanically crushed into several pieces and ground into powders with the stainless mortar in the glove box. The Mg UFPs were produced by HPMR method in a water-cooled chamber connected with a collecting room. The arc discharge of Mg (purity >99.5%) ingot of 20 g was performed in a mixture of hydrogen and argon in a ratio of 1 : 1 with a total pressure of 0.1 MPa. During the process, the discharge current was kept at 100 A. The UFPs were collected in Ar atmosphere. The $(Ti_{0.85}Zr_{0.15})_{1.05}Mn_{1.2}Cr_{0.6}V_{0.1}Cu_{0.1}$ powders and Mg UFPs were mixed homogeneously with a composition of Mg–x wt% $(Ti_{0.85}Zr_{0.15})_{1.05}Mn_{1.2}Cr_{0.6}V_{0.1}Cu_{0.1}$ (x = 0, 5, 10, 30). The mixtures were put into a stainless steel vial in the glove box and were milled under an initial pressure of 4 MPa H_2 with planetary ball miller at a rotation speed of 200 rpm for 2 h and a ball-to-powder ratio of 20 : 1. The collecting and filling of the sample were operated in the glove box filled with Ar to prevent oxidation.

Characterization

The hydrogen absorption and desorption properties of the $(Ti_{0.85}Zr_{0.15})_{1.05}Mn_{1.2}Cr_{0.6}V_{0.1}Cu_{0.1}$ and Mg–x wt% $(Ti_{0.85}Zr_{0.15})_{1.05}Mn_{1.2}Cr_{0.6}V_{0.1}Cu_{0.1}$ (x = 0, 5, 10, 30) composites were evaluated using a Sieverts-type apparatus. Prior to the measurements, the samples of $(Ti_{0.85}Zr_{0.15})_{1.05}Mn_{1.2}Cr_{0.6}V_{0.1}Cu_{0.1}$ alloy experienced one hydrogen absorption/desorption cycle at room temperature at the hydrogen pressure of 4 MPa and vacuum. The Mg–x wt% $(Ti_{0.85}Zr_{0.15})_{1.05}Mn_{1.2}Cr_{0.6}V_{0.1}Cu_{0.1}$ (x = 0, 5, 10, 30) composites were activated by one hydrogen absorption/desorption cycle at 400 °C at the hydrogen pressure of 4 MPa and vacuum. The initial hydrogen pressures for hydrogenation/dehydrogenation were selected as 4 MPa and 100 Pa at each temperature. The pressure–composition–temperature (PCT) curves at different temperatures (623, 648, and 673 K) were plotted using the conventional pressure–volume–temperature technique to investigate the thermodynamic property of the composites. The hydrogen absorption or desorption measurement for the PCT curves was considered as reaching equilibrium when the vibration of hydrogen pressure at the certain temperature was less than 20 Pa s^{-1}. The X-ray diffraction (XRD) patterns of the samples were recorded with a Rigaku X-ray diffractometer with monochromatic Cu Kα radiation. Scanning electronic microscope (SEM) was applied to analyze the morphology of the samples. An energy dispersive spectroscopy (EDS) detector was used to determine the elemental distributions.

Results and discussion

Sample characterization

Fig. 1a displays the typical hexagonal shape of Mg UFPs fabricated by the HPMR method with an average particle size of 300 nm. It can be observed from Fig. 1b that the as-prepared Mg UFPs have single α-Mg phase (JCPDS no. 35-0821, space group $P6_3/mmc$). The as-prepared $(Ti_{0.85}Zr_{0.15})_{1.05}Mn_{1.2}Cr_{0.6}V_{0.1}Cu_{0.1}$ particles consist of single C14-Laves phase (JCPDS no. 50-1114, space group $P6_3/mmc$), see Fig. 1c.

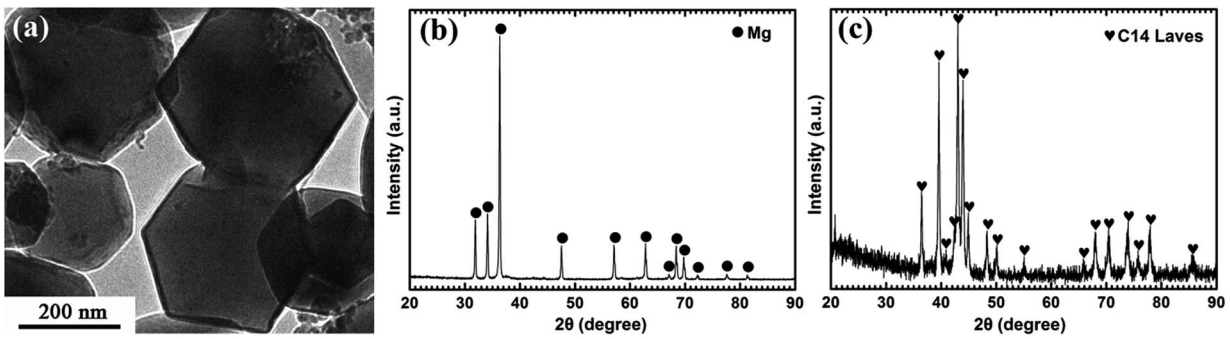

Fig. 1 TEM image of the Mg UFPs fabricated by the HPMR method (a) and XRD patterns of the as-prepared Mg UFPs (b) and $(Ti_{0.85}Zr_{0.15})_{1.05}Mn_{1.2}Cr_{0.6}V_{0.1}Cu_{0.1}$ particles (c).

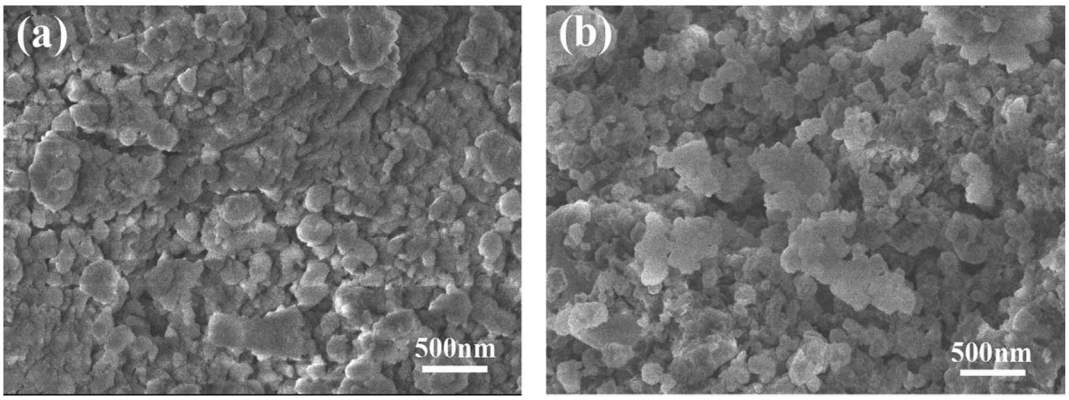

Fig. 2 SEM images of the Mg–30 wt% $(Ti_{0.85}Zr_{0.15})_{1.05}Mn_{1.2}Cr_{0.6}V_{0.1}Cu_{0.1}$ composite: (a) as-milled and (b) after hydrogenation and dehydrogenation cycles.

After ball milling process, the Mg–$TiMn_2$ alloy composites with different percentage of $(Ti_{0.85}Zr_{0.15})_{1.05}Mn_{1.2}Cr_{0.6}V_{0.1}Cu_{0.1}$ show similar morphologies. Fig. 2a displays the SEM image of the as-milled Mg–30 wt% $(Ti_{0.85}Zr_{0.15})_{1.05}Mn_{1.2}Cr_{0.6}V_{0.1}Cu_{0.1}$ composite as an example. It can be seen that the particle size varies from 100 to 500 nm with an average of about 200 nm. The as-milled Mg–$(Ti_{0.85}Zr_{0.15})_{1.05}Mn_{1.2}Cr_{0.6}V_{0.1}Cu_{0.1}$ particles were nearly spherical in shape, which was different from the pure Mg UFPs prepared by HPMR with a clear hexagonal shape (see Fig. 1a). Since $(Ti_{0.85}Zr_{0.15})_{1.05}Mn_{1.2}Cr_{0.6}V_{0.1}Cu_{0.1}$ is brittle, we suppose that the $TiMn_2$ type alloy powders are broken and cover on the Mg UFPs after ball milling. It is interesting to find that the particle size and morphology of the composite sample stay unchangeable after hydrogenation and dehydrogenation cycles, see Fig. 2b.

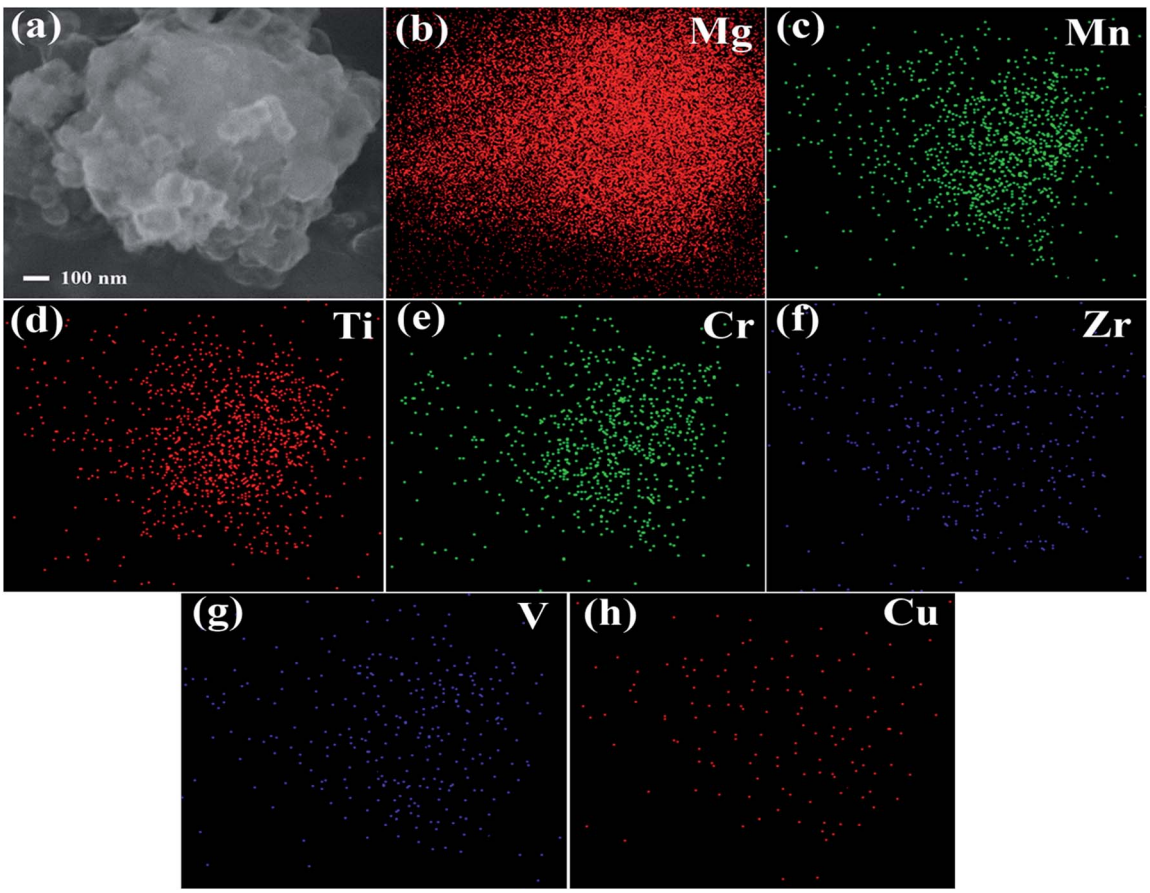

Fig. 3 High magnification SEM image of the Mg–30 wt% $(Ti_{0.85}Zr_{0.15})_{1.05}Mn_{1.2}Cr_{0.6}V_{0.1}Cu_{0.1}$ composite (a) and EDS maps of Mg (b), Mn (c), Ti (d), Cr (e), Zr (f), V (g), Cu (h).

To further reveal the morphology and elements distribution of Mg–$(Ti_{0.85}Zr_{0.15})_{1.05}Mn_{1.2}Cr_{0.6}V_{0.1}Cu_{0.1}$ composite, high magnification SEM and EDS analyses were conducted. Fig. 3a displays the SEM image of Mg–30 wt% $(Ti_{0.85}Zr_{0.15})_{1.05}Mn_{1.2}Cr_{0.6}V_{0.1}Cu_{0.1}$ composite after ball milling. A large number of small particles can be seen clearly on the coarse surface of large particles. EDS mapping results (Fig. 3b–h) show that the composite particle is dominantly made of Mg together with a certain amount of Mn, Ti, Cr, Zr, V, and Cu, which indicates $(Ti_{0.85}Zr_{0.15})_{1.05}Mn_{1.2}Cr_{0.6}V_{0.1}Cu_{0.1}$ particles are distributed homogeneously on the surface of Mg particles. The Mg–$(Ti_{0.85}Zr_{0.15})_{1.05}Mn_{1.2}Cr_{0.6}V_{0.1}Cu_{0.1}$ composites with 5 wt% and 10 wt% $(Ti_{0.85}Zr_{0.15})_{1.05}Mn_{1.2}Cr_{0.6}V_{0.1}Cu_{0.1}$ exhibit similar morphologies and uniform elements distribution.

Fig. 4 shows the XRD patterns of the as-prepared Mg–5 wt% $(Ti_{0.85}Zr_{0.15})_{1.05}Mn_{1.2}Cr_{0.6}V_{0.1}Cu_{0.1}$ composite and the samples obtained after the hydrogen absorption and desorption at 673 K. Three strong diffraction peaks of α-Mg phase at 36.35°, 34.19° and 31.92° can be seen clearly in Fig. 4a, which are in good accordance with the peaks of the as-prepared Mg UFPs sample in Fig. 1b. Four weak diffraction peaks at 39.58°, 43.05°, 43.89° and 44.85° can also be found in Fig. 4a, which agree well with the as-prepared $(Ti_{0.85}Zr_{0.15})_{1.05}Mn_{1.2}Cr_{0.6}V_{0.1}Cu_{0.1}$ alloy with a typical C14 Laves phase (see Fig. 1c). It is known that whether the hydride of Mg can be formed is determined by its hydrogen sorption kinetics and thermodynamics. It was reported that the formation of magnesium hydride during the HPMR process is suppressed by the low hydrogen pressure (0.05 MPa) and the high cooling rate.[31] In this work, no hydride can be found in the XRD pattern of the as-prepared Mg UFPs, see Fig. 1b. Generally, the formation of MgH_2 from Mg by gas–solid reaction needs high temperature (>600 K) and high hydrogen pressure (>5 MPa).[33] Even after milling pure Mg at microscale for 4 h under hydrogen atmosphere, no hydride phase is formed.[34] However, in this work, 4 weak diffraction peaks of MgH_2 (JCPDS no. 12-0697, space group $P4_2/mnm$) at 27.67°, 35.57°, 39.58° and 54.49° for the ball milled pure Mg UFPs are discernable in Fig. S1,† indicating the ultrafine size of Mg particles contributes to the formation of MgH_2 at room temperature. Xie *et al.*[4] also found that hydride can be formed after ball milling under the same condition for Mg UFPs. The intensities of the diffraction peaks of MgH_2 in Mg–5 wt% $(Ti_{0.85}Zr_{0.15})_{1.05}Mn_{1.2}Cr_{0.6}V_{0.1}Cu_{0.1}$ composite in Fig. 4a are even stronger than those in the ball milled pure Mg UFPs. This implies that the catalytic effects of $(Ti_{0.85}Zr_{0.15})_{1.05}Mn_{1.2}Cr_{0.6}V_{0.1}Cu_{0.1}$, together with ultrafine size of Mg particles, is helpful to the formation of more MgH_2. Fan *et al.*[35] also found that $Ti_{0.9}Zr_{0.2}Mn_{1.5}Cr_{0.3}$ alloy catalyzed the reaction between Mg and H_2 at room temperature. There is no $(Ti_{0.85}Zr_{0.15})_{1.05}Mn_{1.2}Cr_{0.6}V_{0.1}Cu_{0.1}$ hydride phase present in the as-prepared XRD patterns. This is due to the fact that the desorption equilibrium pressure of $(Ti_{0.85}Zr_{0.15})_{1.05}Mn_{1.2}Cr_{0.6}V_{0.1}Cu_{0.1}$ is rather high, about 0.9 MPa (see Fig. S2†) at room temperature, thus its hydride phase is not stable during the XRD test.

It can be observed from Fig. 4b that Mg in the Mg–5 wt% $(Ti_{0.85}Zr_{0.15})_{1.05}Mn_{1.2}Cr_{0.6}V_{0.1}Cu_{0.1}$ composite transforms completely into MgH_2 after hydrogenation at 673 K. After the dehydrogenation at 673 K, MgH_2 completely transforms into Mg (see Fig. 4c). The $(Ti_{0.85}Zr_{0.15})_{1.05}Mn_{1.2}Cr_{0.6}V_{0.1}Cu_{0.1}$ phase appears to be stable during the hydrogenation and dehydrogenation process (see Fig. 4b and c), suggesting that $(Ti_{0.85}Zr_{0.15})_{1.05}Mn_{1.2}Cr_{0.6}V_{0.1}Cu_{0.1}$ does not react with Mg, nor does it react with MgH_2. Therefore, the $(Ti_{0.85}Zr_{0.15})_{1.05}Mn_{1.2}Cr_{0.6}V_{0.1}Cu_{0.1}$ dopant plays a role of catalyst during both the hydrogenation and dehydrogenation processes of Mg. Zhou *et al.* also found $Ti_{0.98}Zr_{0.02}V_{0.43}Fe_{0.09}Cr_{0.05}Mn_{1.5}$ phase in Mg–$TiMn_2$ composite stayed stable during the hydrogen absorption and desorption process acting as a catalyst.[36]

Fig. 5a shows that the prepared Mg–10 wt% $(Ti_{0.85}Zr_{0.15})_{1.05}Mn_{1.2}Cr_{0.6}V_{0.1}Cu_{0.1}$ composite also consists of Mg,

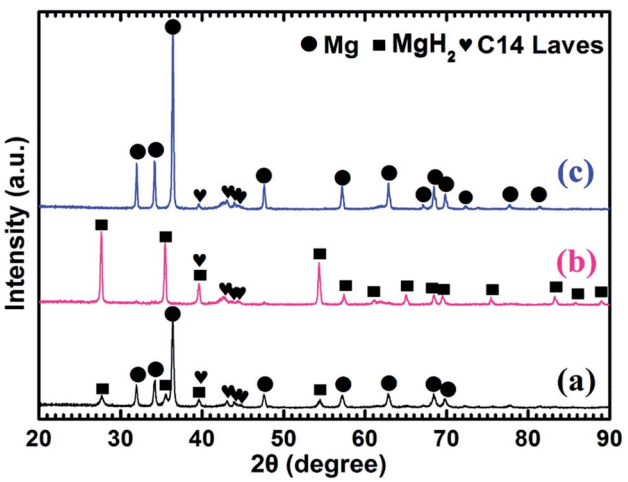

Fig. 4 XRD patterns of the Mg–5 wt% $(Ti_{0.85}Zr_{0.15})_{1.05}Mn_{1.2}Cr_{0.6}V_{0.1}Cu_{0.1}$ composite: (a) as prepared; (b) after the hydrogenation under 4 MPa hydrogen pressure at 673 K; (c) after the dehydrogenation under 100 Pa and at 673 K.

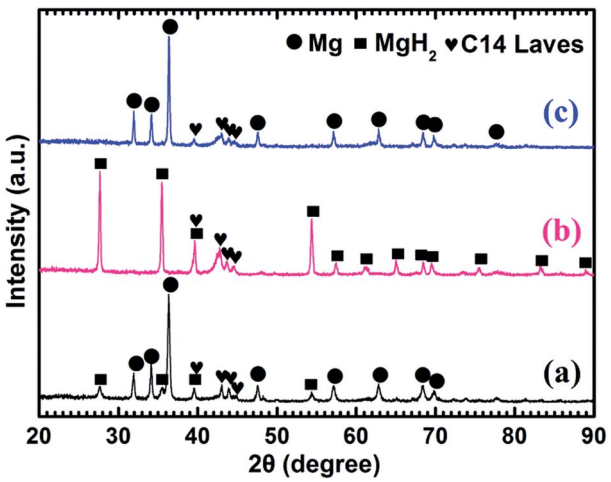

Fig. 5 XRD patterns of the Mg–10 wt% $(Ti_{0.85}Zr_{0.15})_{1.05}Mn_{1.2}Cr_{0.6}V_{0.1}Cu_{0.1}$ composite: (a) as prepared; (b) after the hydrogenation under 4 MPa hydrogen pressure at 673 K; (c) after the dehydrogenation under 100 Pa and at 673 K.

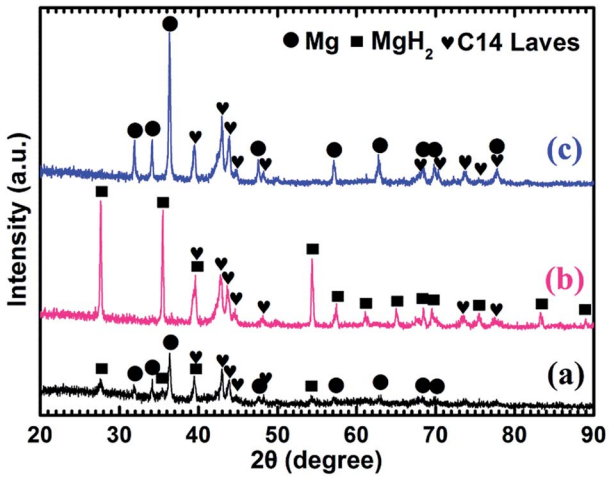

Fig. 6 XRD patterns of the Mg–30 wt% $(Ti_{0.85}Zr_{0.15})_{1.05}Mn_{1.2}Cr_{0.6}V_{0.1}Cu_{0.1}$ composite: (a) as prepared; (b) after the hydrogenation under 4 MPa hydrogen pressure at 673 K; (c) after the dehydrogenation under 100 Pa and at 673 K.

MgH_2 and C14 Laves phases. As shown in Fig. 5b and c, Mg fully transforms into MgH_2 after hydrogenation at 673 K, and MgH_2 releases H_2 completely and transforms into Mg after dehydrogenation at 673 K. The C14-$(Ti_{0.85}Zr_{0.15})_{1.05}Mn_{1.2}Cr_{0.6}V_{0.1}Cu_{0.1}$ phase also keeps stable during the hydrogenation and dehydrogenation process (see Fig. 5b and c). Compared Fig. 4a–c for Mg–5 wt% $(Ti_{0.85}Zr_{0.15})_{1.05}Mn_{1.2}Cr_{0.6}V_{0.1}Cu_{0.1}$ composite, the peak intensities of $(Ti_{0.85}Zr_{0.15})_{1.05}Mn_{1.2}Cr_{0.6}V_{0.1}Cu_{0.1}$-C14 Laves phase in Fig. 5a–c are stronger due to the increasing content.

Fig. 6a represents that the prepared Mg–30 wt% $(Ti_{0.85}Zr_{0.15})_{1.05}Mn_{1.2}Cr_{0.6}V_{0.1}Cu_{0.1}$ composite contains the same phases as the samples with 5 wt% and 10 wt% $TiMn_2$ alloy. Mg transforms into MgH_2 (as shown in Fig. 6b) after absorbing hydrogen at 673 K and then transforms completely into Mg after desorbing hydrogen at 673 K (see Fig. 6c). The $(Ti_{0.85}Zr_{0.15})_{1.05}Mn_{1.2}Cr_{0.6}V_{0.1}Cu_{0.1}$ alloy keeps its phase unchanged during the testing process. It can be seen from Fig. 6 that the intensities of the diffraction peaks of $(Ti_{0.85}Zr_{0.15})_{1.05}Mn_{1.2}Cr_{0.6}V_{0.1}Cu_{0.1}$-C14 Laves phase are much stronger comparing with the composites with 5 wt% and 10 wt% $TiMn_2$ alloy, and more weak peaks such as 48.05°, 73.71° and 77.76° can be seen clear in Fig. 6b and c.

Hydrogen storage properties

To further understand the catalytic effect of $(Ti_{0.85}Zr_{0.15})_{1.05}Mn_{1.2}Cr_{0.6}V_{0.1}Cu_{0.1}$ on the hydrogen properties of Mg, the hydrogen absorption and desorption capacities and kinetics are measured by a carefully calibrated Sieverts-type apparatus. Hydrogen content (wt%) is the weight ratio of hydrogen and the Mg–$(Ti_{0.85}Zr_{0.15})_{1.05}Mn_{1.2}Cr_{0.6}V_{0.1}Cu_{0.1}$ composites. The hydrogenation curves at various temperatures with an initial hydrogen pressure of 4 MPa are presented in Fig. 7. It can be observed from Fig. 7a that the ball milled Mg UFPs can quickly uptake 6.00 wt% hydrogen within 5 min at 673 K and uptake 5.50 wt% hydrogen within 2.5 min at 623 K. However, without milling, the Mg UFPs need 10 min at 673 K and 20 min at 623 K absorb the same amount hydrogen.[31] The ball milled Mg UFPs have hydrogenation capacities of 5.93 wt% at 573 K and 5.83 wt% at 523 K, much higher than that of the Mg UFPs without milling, whose hydrogenation capacities are only 4.82 wt% at 573 K and 4.41 wt% at 523 K.[31] Generally, fresh surface areas can be generated in Mg during the milling process.[35] The higher hydrogenation capacity and better kinetics for the ball milled Mg UFPs are attributed to the fresh surface areas, whose oxide layers may be removed during the milling process.

It is observed in Fig. 7b that Mg–5 wt% $(Ti_{0.85}Zr_{0.15})_{1.05}Mn_{1.2}Cr_{0.6}V_{0.1}Cu_{0.1}$ composite has a high hydrogen absorption capacity of 6.54 wt% and can quickly absorb 6.00 wt% H_2 within 100 s at 673 K, showing better kinetics and capacity than the ball milled pure Mg UFPs, which has a hydrogen absorption capacity of 6.25 wt% and needs 300 s to uptake 6.00 wt% hydrogen at 673 K. This indicates that the $(Ti_{0.85}Zr_{0.15})_{1.05}Mn_{1.2}Cr_{0.6}V_{0.1}Cu_{0.1}$ alloy catalyzes the hydrogenation process of Mg. The reduced particle size of Mg in the Mg–$TiMn_2$ composite compared with Mg UFPs without milling should increase the surface area, which may also attribute to the improved hydrogen storage performance to some extent. On the other hand, the particle sizes of the ball milled Mg with and without $TiMn_2$ alloy are comparable, we suggest that the improved performance of the Mg–x wt% $TiMn_2$ ($x = 5$, 10, 30) samples in comparison with the pure Mg sample after ball milling are mainly attributed to the catalytic effect of $TiMn_2$ alloy. In addition, it takes more than 120 s for Mg–Nb nanocomposite prepared by HPMR to reach a value of 6.00 wt% H_2 under the same condition.[32] It is also observed that the Mg–5 wt% $(Ti_{0.85}Zr_{0.15})_{1.05}Mn_{1.2}Cr_{0.6}V_{0.1}Cu_{0.1}$ composite is able to absorb 6.00 wt% H_2 within 5 min at 623 K, superior to Mg–7 at% Al nanoparticles synthesized by the HPMR method that only absorbed 5.41 wt% H_2 within 5 min at 623 K.[30] These results demonstrate the superior catalytic effects of $(Ti_{0.85}Zr_{0.15})_{1.05}Mn_{1.2}Cr_{0.6}V_{0.1}Cu_{0.1}$ alloy. The Mg–5 wt% $(Ti_{0.85}Zr_{0.15})_{1.05}Mn_{1.2}Cr_{0.6}V_{0.1}Cu_{0.1}$ composite can also rapidly absorb 5.50 wt% H_2 in 5 min and reach a final value of 6.10 wt% at 573 K, higher than the Mg–5 at% $Ti_{0.98}Zr_{0.02}V_{0.43}Fe_{0.09}Cr_{0.05}Mn_{1.5}$ composite prepared by milling commercial MgH_2 (tens micrometer-scale particle size) with $Ti_{0.98}Zr_{0.02}V_{0.43}Fe_{0.09}Cr_{0.05}Mn_{1.5}$ alloy, which absorbed a total of 5.5 wt% H_2 at 573 K.[36] This suggests that the enhanced hydrogenation properties of the Mg–$(Ti_{0.85}Zr_{0.15})_{1.05}Mn_{1.2}Cr_{0.6}V_{0.1}Cu_{0.1}$ composites are also relate to the ultrafine size of Mg which shortens the diffusion distances in the sorption process. The storage capacity of the Mg–5 wt% $(Ti_{0.85}Zr_{0.15})_{1.05}Mn_{1.2}Cr_{0.6}V_{0.1}Cu_{0.1}$ composite reaches 6.00 wt% H_2 within 60 min at 523 K, higher than the Mg–Ti–V nanoparticles which absorbs 5.00 wt% in 60 min at 523 K.[31] The hydrogen absorption capacity of the Mg–5 wt% $(Ti_{0.85}Zr_{0.15})_{1.05}Mn_{1.2}Cr_{0.6}V_{0.1}Cu_{0.1}$ composite decreases dramatically from 3.78 wt% to 0.68 wt% with the temperature dropping from 473 K to 423 K, which is still much higher than that of the ball milled pure Mg UFPs which only absorb 1.47 wt% and 0.06 wt% H_2 at 473 K and 423 K respectively (see Fig. 7a).

It can be seen from Fig. 7c that the Mg–10 wt% $(Ti_{0.85}Zr_{0.15})_{1.05}Mn_{1.2}Cr_{0.6}V_{0.1}Cu_{0.1}$ composite has hydrogenation capacities of 5.72, 5.52, 5.14, 4.69 and 2.90 wt% H_2 at 673, 623,

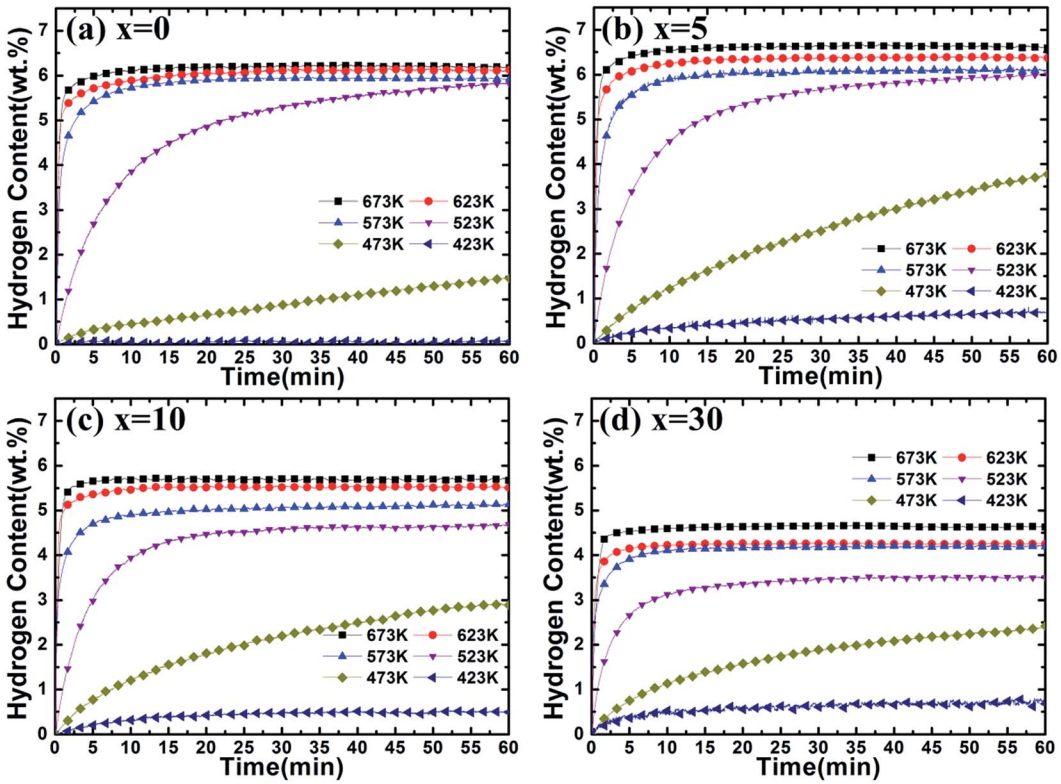

Fig. 7 Hydrogenation kinetics of Mg–x wt% $(Ti_{0.85}Zr_{0.15})_{1.05}Mn_{1.2}Cr_{0.6}V_{0.1}Cu_{0.1}$ (x = 0, 5, 10, 30) composites at 4 MPa hydrogen and different temperatures.

573, 523 and 473 K respectively, lower than that of the Mg–5 wt% $(Ti_{0.85}Zr_{0.15})_{1.05}Mn_{1.2}Cr_{0.6}V_{0.1}Cu_{0.1}$ composite. That is due to $(Ti_{0.85}Zr_{0.15})_{1.05}Mn_{1.2}Cr_{0.6}V_{0.1}Cu_{0.1}$ alloy does not absorb or desorb hydrogen at the temperature above 423 K (as shown in Fig. S3†). The reaction percentage (%) for certain reaction time is calculated through dividing the hydrogen content for the reaction time by the saturation hydrogen content at different temperatures. The hydrogenation reaction percentage of Mg–10 wt% $(Ti_{0.85}Zr_{0.15})_{1.05}Mn_{1.2}Cr_{0.6}V_{0.1}Cu_{0.1}$ composite within 10 min is calculated from Fig. 7c to be 84% and 41% at 523 K and 473 K respectively. However, the hydrogenation reaction percentage of the Mg–5 wt% $(Ti_{0.85}Zr_{0.15})_{1.05}Mn_{1.2}Cr_{0.6}V_{0.1}Cu_{0.1}$ composite within 10 min calculated from Fig. 7b is only 75% and 32% at 523 K and 473 K respectively, indicating that the increase of $(Ti_{0.85}Zr_{0.15})_{1.05}Mn_{1.2}Cr_{0.6}V_{0.1}Cu_{0.1}$ content contributes to the improvement of hydrogenation kinetics.

Fig. 7d shows that the Mg–30 wt% $(Ti_{0.85}Zr_{0.15})_{1.05}Mn_{1.2}Cr_{0.6}V_{0.1}Cu_{0.1}$ composite can absorb 4.63, 4.25, 4.19, 3.50 and 2.41 wt% H_2 at 673, 623, 573, 523 and 473 K respectively, lower than the composite with 10 wt% $(Ti_{0.85}Zr_{0.15})_{1.05}Mn_{1.2}Cr_{0.6}V_{0.1}Cu_{0.1}$ because of the increasing weight of $(Ti_{0.85}Zr_{0.15})_{1.05}Mn_{1.2}Cr_{0.6}V_{0.1}Cu_{0.1}$ alloy. It can be calculated from Fig. 7b that the hydrogenation reaction percentage of the Mg–30 wt% $(Ti_{0.85}Zr_{0.15})_{1.05}Mn_{1.2}Cr_{0.6}V_{0.1}Cu_{0.1}$ composite at 10 min is 91% and 47% at 523 K and 473 K respectively, better than the composite with 10 wt% $(Ti_{0.85}Zr_{0.15})_{1.05}Mn_{1.2}Cr_{0.6}V_{0.1}Cu_{0.1}$ alloy. This implies that $(Ti_{0.85}Zr_{0.15})_{1.05}Mn_{1.2}Cr_{0.6}V_{0.1}Cu_{0.1}$ improves the hydrogenation kinetics of Mg, and adding more $(Ti_{0.85}Zr_{0.15})_{1.05}Mn_{1.2}Cr_{0.6}V_{0.1}Cu_{0.1}$ leads to higher hydrogenation rate but deteriorates hydrogenation capacity.

It can be concluded that adding a certain amount of $(Ti_{0.85}Zr_{0.15})_{1.05}Mn_{1.2}Cr_{0.6}V_{0.1}Cu_{0.1}$ alloy can improve both the hydrogen absorption capacity and rate of Mg. The hydrogen absorption capacity of the Mg–$(Ti_{0.85}Zr_{0.15})_{1.05}Mn_{1.2}Cr_{0.6}V_{0.1}Cu_{0.1}$ composite decreases but its kinetics improves with the increase of $(Ti_{0.85}Zr_{0.15})_{1.05}Mn_{1.2}Cr_{0.6}V_{0.1}Cu_{0.1}$ content.

The dehydrogenation curves of Mg–x wt% $(Ti_{0.85}Zr_{0.15})_{1.05}Mn_{1.2}Cr_{0.6}V_{0.1}Cu_{0.1}$ (x = 0, 5, 10, 30) composites at various temperatures with an initial hydrogen pressure of 100 Pa are presented in Fig. 8. It is observed that the ball milled Mg UFPs can release 5.00 wt% H_2 in 2 min at 673 K and reach a value of 6.20 wt% H_2 in 60 min, much better than the Mg UFPs without milling, which can only desorb less than 5.00 wt% H_2 within 60 min at the same temperature.[31] It is also observed that the ball milled Mg UFPs can quickly desorb 6.00 wt% H_2 in 20 min and reach a value of 6.10 wt% H_2 in 60 min at 623 K, superior to the Mg UFPs synthesized by the HPMR method that released less than 4.00 wt% H_2 at 623 K in 60 min.[31] Obviously, the milling process significantly improves the dehydrogenation capacities and kinetics of Mg.

As shown in Fig. 8b, Mg–5 wt% $(Ti_{0.85}Zr_{0.15})_{1.05}Mn_{1.2}Cr_{0.6}V_{0.1}Cu_{0.1}$ composite is able to quickly desorb 6.00 wt% H_2 within 90 s at 673 K and within 15 min at 623 K, while it takes 250 s and 20 min for the ball milled Mg UFPs to reach the same value at 673 K and 623 K respectively, indicating that the $(Ti_{0.85}Zr_{0.15})_{1.05}Mn_{1.2}Cr_{0.6}V_{0.1}Cu_{0.1}$ alloy improves the hydrogen

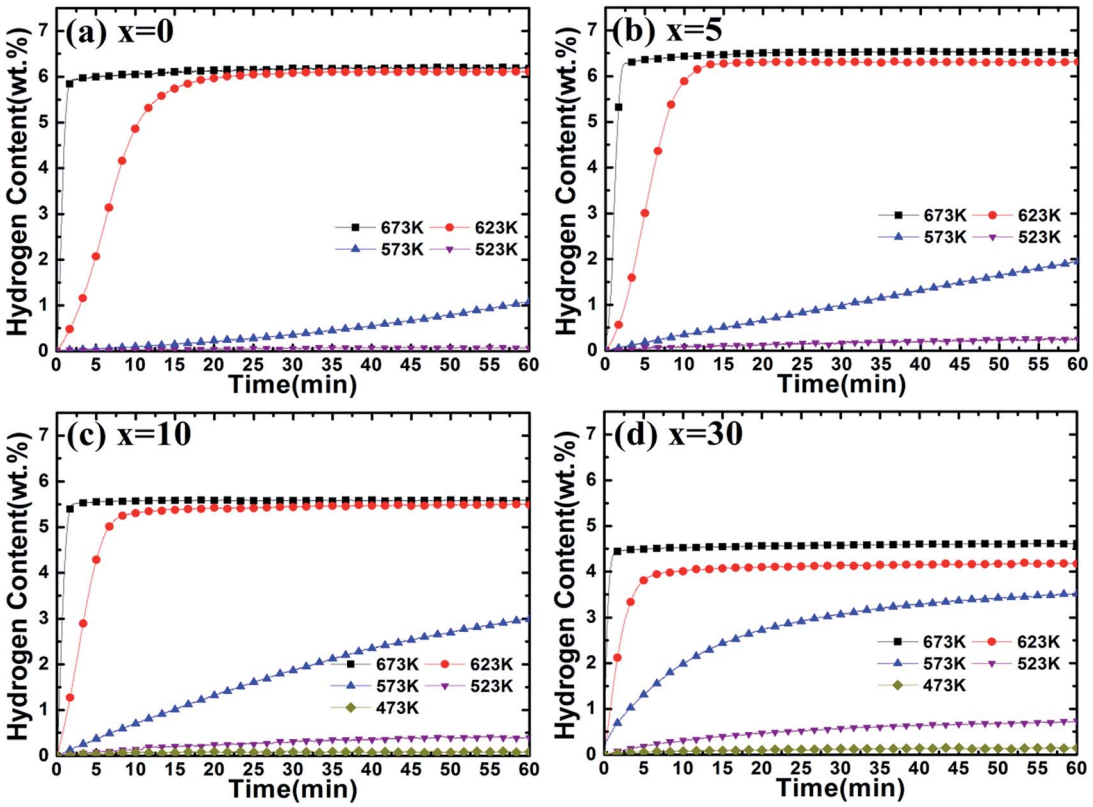

Fig. 8 Dehydrogenation kinetics of Mg–x wt% $(Ti_{0.85}Zr_{0.15})_{1.05}Mn_{1.2}Cr_{0.6}V_{0.1}Cu_{0.1}$ (x = 0, 5, 10, 30) composites at 100 Pa and different temperatures.

desorption capacities and kinetics apparently as a catalyst. In comparison with the Mg–Nb nanocomposite which needed 220 s to desorb 6.00 wt% H_2 at 673 K and 27 min to desorb 6.00 wt% H_2 at 673 K,[32] the $(Ti_{0.85}Zr_{0.15})_{1.05}Mn_{1.2}Cr_{0.6}V_{0.1}Cu_{0.1}$ alloy shows superior catalytic effects on the dehydrogenation of MgH_2. The hydrogen desorption capacity of Mg–5 wt% $(Ti_{0.85}Zr_{0.15})_{1.05}Mn_{1.2}Cr_{0.6}V_{0.1}Cu_{0.1}$ composite within 60 min reaches 6.51 wt% H_2 at 673 K, 6.30 wt% H_2 at 623 K and 1.93 wt% H_2 at 573 K, much higher than that of Mg–Ti–V nanocomposite which desorbed 5.01 wt%, 4.02 wt% and 1.13 wt% H_2 at 673 K, 623 K and 573 K respectively.[31] It can be deduced that the $(Ti_{0.85}Zr_{0.15})_{1.05}Mn_{1.2}Cr_{0.6}V_{0.1}Cu_{0.1}$ particles on the surface of MgH_2 particles effectively improve the hydrogen desorption rate and capacity of MgH_2. It can be seen from Fig. 8c that the Mg–10 wt% $(Ti_{0.85}Zr_{0.15})_{1.05}Mn_{1.2}Cr_{0.6}V_{0.1}Cu_{0.1}$ composite has dehydrogenation capacities of 5.59 wt% H_2 at 673 K and 5.50 wt% H_2 at 623 K, lower than that of the Mg–5 wt% $(Ti_{0.85}Zr_{0.15})_{1.05}Mn_{1.2}Cr_{0.6}V_{0.1}Cu_{0.1}$ composite due to the dead weight of $(Ti_{0.85}Zr_{0.15})_{1.05}Mn_{1.2}Cr_{0.6}V_{0.1}Cu_{0.1}$ alloy. The Mg–10 wt% $(Ti_{0.85}Zr_{0.15})_{1.05}Mn_{1.2}Cr_{0.6}V_{0.1}Cu_{0.1}$ composite can desorb 2.99 wt% H_2 within 200 s at 623 K, whose dehydrogenation reaction percentage at 200 s calculated from Fig. 8c is 54.4%. In comparison, the Mg–5 wt% $(Ti_{0.85}Zr_{0.15})_{1.05}Mn_{1.2}Cr_{0.6}V_{0.1}Cu_{0.1}$ composite can desorb 1.17 wt% H_2 within 200 s at 623 K, whose dehydrogenation reaction percentage at 200 s calculated from Fig. 8b is only 18.1%, indicating the increase of $(Ti_{0.85}Zr_{0.15})_{1.05}Mn_{1.2}Cr_{0.6}V_{0.1}Cu_{0.1}$ content contributes to the improvement of its dehydrogenation kinetics. Surprisingly, the Mg–10 wt% $(Ti_{0.85}Zr_{0.15})_{1.05}Mn_{1.2}Cr_{0.6}V_{0.1}Cu_{0.1}$ composite can release 2.99 wt% H_2 within 60 min at 573 K, much higher than the Mg–5 wt% $(Ti_{0.85}Zr_{0.15})_{1.05}Mn_{1.2}Cr_{0.6}V_{0.1}Cu_{0.1}$ composite of 1.93 wt% under the same condition despite the increase of the dead weight of $(Ti_{0.85}Zr_{0.15})_{1.05}Mn_{1.2}Cr_{0.6}V_{0.1}Cu_{0.1}$ alloy. The similar phenomenon happens at 523 K. As shown in Fig. S3b,† the $(Ti_{0.85}Zr_{0.15})_{1.05}Mn_{1.2}Cr_{0.6}V_{0.1}Cu_{0.1}$ alloy has higher capacities and faster reaction rate during the hydrogen desorption process with the temperature decreases, which may cause its more significant catalytic effects on Mg at lower temperatures and thus lead to the unique phenomenon that Mg–$(Ti_{0.85}Zr_{0.15})_{1.05}Mn_{1.2}Cr_{0.6}V_{0.1}Cu_{0.1}$ composites have better hydrogen desorption capacities and kinetics at relatively low temperatures (<573 K) with the increasing content of $(Ti_{0.85}Zr_{0.15})_{1.05}Mn_{1.2}Cr_{0.6}V_{0.1}Cu_{0.1}$.

Fig. 8d represents that the Mg–30 wt% $(Ti_{0.85}Zr_{0.15})_{1.05}Mn_{1.2}Cr_{0.6}V_{0.1}Cu_{0.1}$ composite can release 4.62 wt% H_2 at 673 K and 4.18 wt% H_2 at 623 K, lower than the Mg–10 $(Ti_{0.85}Zr_{0.15})_{1.05}Mn_{1.2}Cr_{0.6}V_{0.1}Cu_{0.1}$ wt% composite with less $TiMn_2$ alloy. However, the Mg–30 wt% $(Ti_{0.85}Zr_{0.15})_{1.05}Mn_{1.2}Cr_{0.6}V_{0.1}Cu_{0.1}$ composite still shows better dehydrogenation kinetics than Mg–10 wt% $(Ti_{0.85}Zr_{0.15})_{1.05}Mn_{1.2}Cr_{0.6}V_{0.1}Cu_{0.1}$ composite. It can desorb 3.35 wt% H_2 within 200 s at 623 K, whose reaction percentage at 200 s calculated from Fig. 8d is 80.2% (54.4% for Mg–10 wt% $(Ti_{0.85}Zr_{0.15})_{1.05}Mn_{1.2}Cr_{0.6}V_{0.1}Cu_{0.1}$ composite). At 573 K and 523 K, the Mg–30 wt% $(Ti_{0.85}Zr_{0.15})_{1.05}Mn_{1.2}Cr_{0.6}V_{0.1}Cu_{0.1}$

composite can release 3.52 wt% and 0.73 wt% H_2 within 60 min respectively, higher than Mg–10 wt% $(Ti_{0.85}Zr_{0.15})_{1.05}Mn_{1.2}Cr_{0.6}V_{0.1}Cu_{0.1}$ composite which can only desorb 2.99 wt% and 0.40 wt% H_2 under the same temperatures. This further supports the fact that $(Ti_{0.85}Zr_{0.15})_{1.05}Mn_{1.2}Cr_{0.6}V_{0.1}Cu_{0.1}$ alloy plays an important role in promoting the hydrogen desorption properties of Mg.

In conclusion, we can find that both the hydrogen desorption capacity and rate of Mg are improved by the addition of a certain amount of $(Ti_{0.85}Zr_{0.15})_{1.05}Mn_{1.2}Cr_{0.6}V_{0.1}Cu_{0.1}$ alloy. With the increase of $(Ti_{0.85}Zr_{0.15})_{1.05}Mn_{1.2}Cr_{0.6}V_{0.1}Cu_{0.1}$ content, the hydrogen desorption kinetics of the composites improves but their capacity decreases at the temperature above 573 K. Specifically, both the hydrogen desorption kinetics and capacity of the composites increase with the enlargement of the $(Ti_{0.85}Zr_{0.15})_{1.05}Mn_{1.2}Cr_{0.6}V_{0.1}Cu_{0.1}$ alloy content at the temperature below 573 K.

The JMAK (Johnson–Mehl–Avrami–Kolmogorov) model is used to express the hydrogen sorption kinetics (see eqn (1)):[37]

$$\ln[-\ln(1-\alpha)] = \eta \ln k + \eta \ln t \quad (1)$$

where k is the reaction rate constant, η is the Avrami exponent of reaction order, and α is the fraction transformed at time t. For each temperature, the slope η and the intercept $\eta \ln(k)$ can be obtained from the plot of $\ln[-\ln(1-\alpha)]$ *vs.* $\ln(t)$.

Then, the Arrhenius equation is used to calculate the hydrogenation activation energy:[38,39]

$$k = A \exp(-E_a/RT) \quad (2)$$

where R is the gas constant (8.314472 J mol^{-1} K^{-1}), T represents the absolute temperature, E_a is the activation energy, k is the rate constant and A is the pre-exponential factor, a constant. The hydrogenation activation energy of the ball milled Mg UFPs calculated from Fig. 9a is 81.71 kJ mol^{-1}, much smaller than Mg UFPs prepared by HPMR without milling of 123.8 kJ mol^{-1},[31] demonstrating the milling process lowers the hydrogenation activation energy effectively. The hydrogenation activation energies of the composite samples decrease with increasing $(Ti_{0.85}Zr_{0.15})_{1.05}Mn_{1.2}Cr_{0.6}V_{0.1}Cu_{0.1}$ content. E_a values of the composites with 5, 10, 30 wt% $TiMn_2$ alloy are calculated to be 67.52, 65.80, 60.99 kJ mol^{-1} respectively, see Fig. 9a, much smaller than the ball milled Mg particles. This implies $(Ti_{0.85}Zr_{0.15})_{1.05}Mn_{1.2}Cr_{0.6}V_{0.1}Cu_{0.1}$ can reduce the hydrogenation activation energy of Mg effectively. They are also smaller than Mg–Nb nanocomposite of 70.9 kJ mol^{-1},[32] indicating the superior catalytic effect of $(Ti_{0.85}Zr_{0.15})_{1.05}Mn_{1.2}Cr_{0.6}V_{0.1}Cu_{0.1}$. The hydrogenation activation energy of Mg (microsize)–$Ti_{0.98}Zr_{0.02}V_{0.43}Fe_{0.09}Cr_{0.05}Mn_{1.5}$ composite is 74.22 kJ mol^{-1}, higher than those composites in this work.[36] This suggests that the ultrafine size of Mg particles may also help decrease its hydrogenation activation energy.

The dehydrogenation activation energy of the ball milled Mg UFPs calculated from Fig. 9b is 124.75 kJ mol^{-1}, smaller than Mg UFPs prepared by HPMR without milling process of 127.7 kJ mol^{-1},[31] demonstrating the milling process lowers the dehydrogenation activation energy. The hydrogenation activation energies of the composite samples also decrease with increasing $(Ti_{0.85}Zr_{0.15})_{1.05}Mn_{1.2}Cr_{0.6}V_{0.1}Cu_{0.1}$ content. E_a values of the composites with 5, 10, 30 wt% $TiMn_2$ alloy calculated from Fig. 9a are 121.37, 116.68, 77.52 kJ mol^{-1}, respectively, smaller than the ball milled Mg particles of 124.75 kJ mol^{-1} (see Fig. 9b). This implies adding $(Ti_{0.85}Zr_{0.15})_{1.05}Mn_{1.2}Cr_{0.6}V_{0.1}Cu_{0.1}$ can reduce the dehydrogenation activation energy of Mg effectively. The dehydrogenation activation energy of the composite with 30 wt% $TiMn_2$ alloy is lower than that of the Mg–7 at% Al composite of 105.5 kJ mol^{-1} (ref. 30) and the Mg–Nb nanocomposite of 86.4 kJ mol^{-1},[32] demonstrating the superior catalytic effect of $(Ti_{0.85}Zr_{0.15})_{1.05}Mn_{1.2}Cr_{0.6}V_{0.1}Cu_{0.1}$.

Because of the absence of d-electrons orbital, Mg does not have sufficient ability to dissociate hydrogen molecules without catalytic additives. In this work, $(Ti_{0.85}Zr_{0.15})_{1.05}Mn_{1.2}Cr_{0.6}V_{0.1}Cu_{0.1}$ particles make it easier for H_2 molecules to be split into hydrogen atoms through facilitating the dissociation of hydrogen gas molecules during the hydrogenation process.[36] When the dehydrogenation begins, some hydrogen atoms will be released from the MgH_2 at the interface of MgH_2/$(Ti_{0.85}Zr_{0.15})_{1.05}Mn_{1.2}Cr_{0.6}V_{0.1}Cu_{0.1}$ in priority because of destabilization of Mg–H bond by the $TiMn_2$ alloy.[33] As we can see in

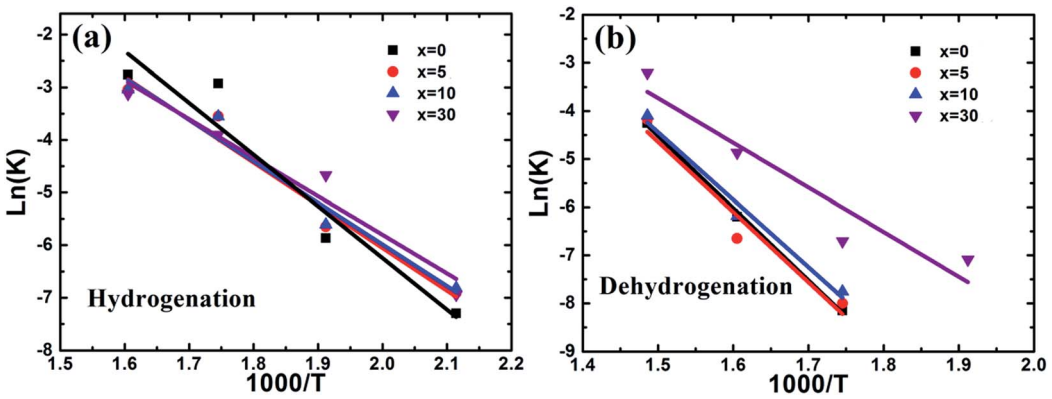

Fig. 9 Plots of ln k *vs.* 1000/T for the hydrogenation (a) and dehydrogenation (b) of the Mg–x wt% $(Ti_{0.85}Zr_{0.15})_{1.05}Mn_{1.2}Cr_{0.6}V_{0.1}Cu_{0.1}$ (x = 0, 5, 10, 30) composites.

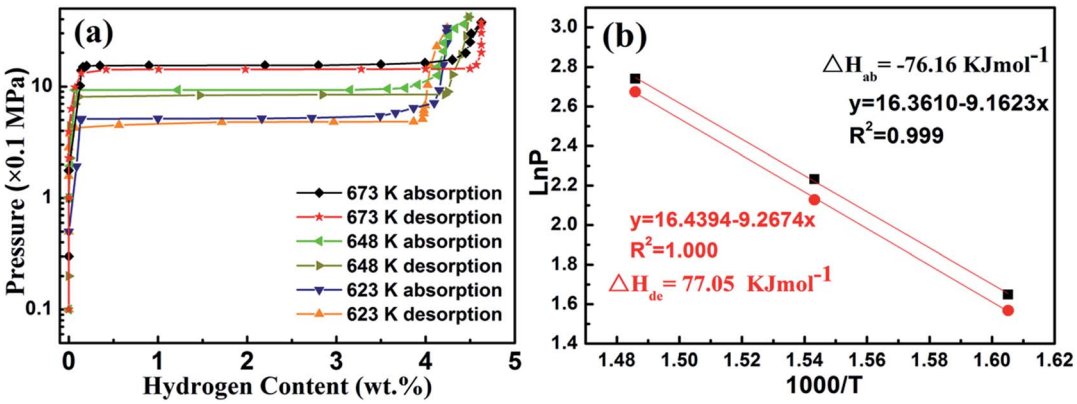

Fig. 10 *P–C* isotherm curves at 623, 648, and 673 K (a) and Van't Hoff plots (b) for the Mg–30 wt% $(Ti_{0.85}Zr_{0.15})_{1.05}Mn_{1.2}Cr_{0.6}V_{0.1}Cu_{0.1}$ composite.

Fig. S3,† the hydride of $(Ti_{0.85}Zr_{0.15})_{1.05}Mn_{1.2}Cr_{0.6}V_{0.1}Cu_{0.1}$ cannot exist stably at the temperature above 423 K. Hydrogen atoms will therefore be recombined and released in the form of hydrogen molecules immediately once they are generated at the interface. The reduction of H_2 accelerates the reaction: $MgH_2 = Mg + H_2$, thus the dehydrogenation kinetics will be enhanced. Additionally, the interfaces at the $(Ti_{0.85}Zr_{0.15})_{1.05}Mn_{1.2}Cr_{0.6}V_{0.1}Cu_{0.1}/MgH_2$ boundaries with high interfacial energy can act as fast hydrogen diffusion paths to accelerate the hydrogen desorption process of MgH_2.[32]

Mg–30 wt% $(Ti_{0.85}Zr_{0.15})_{1.05}Mn_{1.2}Cr_{0.6}V_{0.1}Cu_{0.1}$ composite was selected to evaluate the thermodynamic effects of the $(Ti_{0.85}Zr_{0.15})_{1.05}Mn_{1.2}Cr_{0.6}V_{0.1}Cu_{0.1}$ alloy on Mg. The PCT curves of the hydrogen absorption/desorption at 623, 648, and 673 K are plotted in Fig. 10a. Since the $(Ti_{0.85}Zr_{0.15})_{1.05}Mn_{1.2}Cr_{0.6}V_{0.1}Cu_{0.1}$ does not absorb hydrogen at the testing temperatures, only one flat plateau is detected for each absorption/desorption process as a result of the transformation between Mg and MgH_2 at each temperature. The hydrogen equilibrium pressures of the absorption plateaus are 1.55 MPa at 673 K, 0.93 MPa at 648 K, and 0.52 MPa at 623 K. By plotting the logarithm of the equilibrium pressures $\ln(P)$ against the inverse temperature $1000/T$ and drawing the fitting line according to these plots, the Van't Hoff equation for absorption is determined as $\ln(P) = -9.162/T + 16.361$. The formation enthalpy (ΔH_{ab}) calculated accordingly for the Mg–30 wt% $(Ti_{0.85}Zr_{0.15})_{1.05}Mn_{1.2}Cr_{0.6}V_{0.1}Cu_{0.1}$ composite is −76.16 kJ mol^{-1}, which is comparable to the reported enthalpy value for MgH_2 (−75 kJ mol^{-1}).[40] The hydrogen equilibrium pressures of the desorption plateaus are 1.45 MPa at 673 K, 0.84 MPa at 648 K, and 0.48 MPa at 623 K. The Van't Hoff equation for desorption is $\ln(P) = -9.2674/T + 16.439$. The decomposition enthalpy (ΔH_{de}) for the Mg–30 wt% $(Ti_{0.85}Zr_{0.15})_{1.05}Mn_{1.2}Cr_{0.6}V_{0.1}Cu_{0.1}$ composite is evaluated to be 77.05 kJ mol^{-1}. Thus, the addition of $(Ti_{0.85}Zr_{0.15})_{1.05}Mn_{1.2}Cr_{0.6}V_{0.1}Cu_{0.1}$ does not apparently change the thermodynamics of hydrogenation and dehydrogenation of Mg. The high hydrogen storage capacity and the enhanced hydrogen sorption kinetics are due to the catalytic effect of $(Ti_{0.85}Zr_{0.15})_{1.05}Mn_{1.2}Cr_{0.6}V_{0.1}Cu_{0.1}$ alloys and the ultrafine size of Mg.

Conclusions

The Mg–*x* wt% $(Ti_{0.85}Zr_{0.15})_{1.05}Mn_{1.2}Cr_{0.6}V_{0.1}Cu_{0.1}$ (x = 0, 5, 10, 30) composites have been successfully prepared by ball milling. The $(Ti_{0.85}Zr_{0.15})_{1.05}Mn_{1.2}Cr_{0.6}V_{0.1}Cu_{0.1}$ particles are homogeneously distributed on the surface or embedded in the Mg UFPs. Adding $(Ti_{0.85}Zr_{0.15})_{1.05}Mn_{1.2}Cr_{0.6}V_{0.1}Cu_{0.1}$ alloy contributes to the enhanced hydrogen storage capacities and kinetics. Mg–5 wt% $(Ti_{0.85}Zr_{0.15})_{1.05}Mn_{1.2}Cr_{0.6}V_{0.1}Cu_{0.1}$ composite can uptake 6.00 wt% H_2 within 60 min at 523 K. It can release 6.00 wt% H_2 within 15 min at 623 K. Both the hydrogen absorption and desorption kinetics of the composites improve when the content of $(Ti_{0.85}Zr_{0.15})_{1.05}Mn_{1.2}Cr_{0.6}V_{0.1}Cu_{0.1}$ grows. E_a values of the composites with 0, 5, 10, 30 wt% $TiMn_2$ alloy for hydrogenation and dehydrogenation are 81.71, 67.52, 65.80, 60.99 kJ mol^{-1} and 124.75, 121.37, 116.68, 77.25 kJ mol^{-1}, respectively. The ultrafine size of Mg and the catalytic effect of $(Ti_{0.85}Zr_{0.15})_{1.05}Mn_{1.2}Cr_{0.6}V_{0.1}Cu_{0.1}$ particles give rise to the improved hydrogen storage capacities and kinetics.

Acknowledgements

The authors acknowledge the support of this work by the Joint Fund of the National Natural Science Foundation of China and Baosteel Group Corporation (No. U1560106), the Aeronautical Science Foundation of China (No. 2016ZF51050) and the Scientific Research Foundation for the Returned Overseas Chinese Scholars (State Education Ministry).

References

1 C. Weidenthaler and M. Felderhoff, *Energy Environ. Sci.*, 2011, **4**, 2495–2502.
2 H. Y. Shao, T. Liu and X. G. Li, *Nanotechnology*, 2003, **14**, L1–L3.
3 Y. P. Pang, Y. F. Liu, X. Zhang, Y. Li, M. X. Gao and H. G. Pan, *RSC Adv.*, 2015, **5**, 12144–12151.
4 X. B. Xie, X. J. Ma, P. Liu, J. X. Shang, X. G. Li and T. Liu, *ACS Appl. Mater. Interfaces*, 2017, **9**, 5937–5946.

5 T. Liu, H. L. Shen, Y. Liu, L. Xie, J. L. Qu, H. Y. Shao and X. G. Li, *J. Power Sources*, 2013, **227**, 86–93.
6 H. Emami, K. Edalati, A. Staykov, T. Hongo, H. Iwaoka, Z. Horita and E. Akiba, *RSC Adv.*, 2016, **6**, 11665–11674.
7 L. Xie, J. Li, T. Zhang, L. Song and H. Kou, *J. Power Sources*, 2017, **338**, 91–102.
8 T. Liu, Y. R. Cao, C. G. Qin, W. S. Chou and X. G. Li, *J. Power Sources*, 2014, **246**, 277–282.
9 S. Milošević, S. Kurko, L. Pasquini, L. Matović, R. Vujasin and N. Novaković, *J. Power Sources*, 2016, **307**, 481–488.
10 N. Juahir, N. S. Mustafa, A. M. Sinin and M. Ismail, *RSC Adv.*, 2015, **5**, 60983–60989.
11 G. Barkhordarian, T. Klassen and R. Bormann, *Scr. Mater.*, 2003, **49**, 213–217.
12 N. Hanada, T. Ichikawa, S. Hino and H. Fujii, *J. Alloys Compd.*, 2006, **420**, 46–49.
13 T. Kimura, H. Miyaoka, T. Ichikawa and Y. Kojima, *Int. J. Hydrogen Energy*, 2013, **38**, 13728–13733.
14 T. Liu, C. G. Chen, C. G. Qin and X. G. Li, *Int. J. Hydrogen Energy*, 2014, **39**, 18273–18279.
15 N. Mahmoudi, A. Kaflou and A. Simchi, *J. Power Sources*, 2011, **196**, 4604–4608.
16 A. Zaluska, L. Zaluski and J. O. Strom-Olsen, *J. Alloys Compd.*, 1999, **288**, 217–225.
17 B. Zahiri, M. Danaie, X. H. Tan, B. S. Amirkhiz, G. A. Botton and D. Mitlin, *J. Phys. Chem. C*, 2012, **116**, 3188–3199.
18 Y. Q. Hu, C. Yan, H. F. Zhang, L. Ye and Z. Q. Hu, *J. Alloys Compd.*, 2003, **354**, 296–302.
19 X. Liu, Z. Huang, L. Jiang and S. Wang, *Int. J. Hydrogen Energy*, 2007, **32**, 965–968.
20 E. Grigorova, M. Khristov, M. Khrussanova and P. Peshev, *J. Mater. Sci.*, 2008, **43**, 5336–5341.
21 B. H. Liu, D. M. Kim and K. Y. Lee, *J. Alloys Compd.*, 1996, **240**, 214–218.
22 H. Y. Shao, J. Matsuda, H. Y. Li, E. Akiba, A. Jain, T. Ichikawa and Y. Kojima, *Int. J. Hydrogen Energy*, 2013, **38**, 7070–7076.
23 J. Lu, Y. J. Choi, Z. Z. Fang, H. Y. Sohn and E. Rönnebro, *J. Am. Chem. Soc.*, 2010, **132**, 6616–6617.
24 H. Y. Shao, G. B. Xin, J. Zheng, X. G. Li and E. Akiba, *Nano Energy*, 2012, **1.4**, 590–601.
25 R. W. P. Wagemans, J. H. Van Lenthe, P. E. De Jongh, A. J. Van Dillen and K. P. De Jong, *J. Am. Chem. Soc.*, 2005, **127**, 16675–16680.
26 P. E. Jongh and P. Adelhelm, *ChemSusChem*, 2010, **3**, 1332–1348.
27 K. J. Jeon, H. R. Moon, A. M. Ruminski, B. Jiang, C. Kisielowski, R. Bardhan and J. Urban, *Nat. Mater.*, 2011, **10**, 286–290.
28 K. F. Aguey-Zinsou and J. R. Ares-Fernández, *Chem. Mater.*, 2008, **20**, 376–378.
29 R. Bardhan, A. M. Ruminski, A. Brand and J. Urban, *Energy Environ. Sci.*, 2011, **4**, 4882–4895.
30 T. Liu, C. G. Qin, T. W. Zhang, Y. R. Cao, M. Zhu and X. G. Li, *J. Mater. Chem.*, 2012, **22**, 19831–19838.
31 T. Liu, C. G. Chen, H. Wang and Y. Wu, *J. Phys. Chem. C*, 2014, **118**, 22419–22425.
32 T. Liu, X. J. Ma, C. G. Chen, L. Xu and X. G. Li, *J. Phys. Chem. C*, 2015, **119**, 14029–14037.
33 M. Bortz, B. Bertheville, G. Bottger and K. Yvon, *J. Alloys Compd.*, 1999, **287**, 1–2.
34 Y. Q. Hu, H. F. Zhang, A. M. Wang, B. Z. Ding and Z. Q. Hu, *J. Alloys Compd.*, 2003, **354**, 296–302.
35 M. Q. Fan, L. X. Sun and F. Xu, *Trans. Nonferrous Met. Soc. China*, 2010, **20**, 1447–1451.
36 C. S. Zhou, Z. Z. Fang, C. Ren, J. Z. Li and J. Lu, *J. Phys. Chem. C*, 2013, **117**, 12973–12980.
37 T. R. Jensen, A. Andreasen, T. Vegge, J. W. Andreasen, K. Ståhl, A. S. Pedersen, M. M. Nielsen, A. M. Molenbroek and F. Besenbacher, *Int. J. Hydrogen Energy*, 2006, **31**, 2052–2062.
38 T. He, Z. T. Xiong, G. T. Wu, H. L. Chu, C. Z. Wu, T. Zhang and P. Chen, *Chem. Mater.*, 2009, **21**, 2315–2318.
39 Y. J. Choi, J. W. Choi, H. Y. Sohn, T. Ryu, K. S. Hwang and Z. Z. Fang, *Int. J. Hydrogen Energy*, 2009, **34**, 7700–7706.
40 J. F. Stampfer, C. E. Holley and J. F. Suttle, *J. Am. Chem. Soc.*, 1960, **82**, 3504–3508.